A multiquery analysis of a PeWEC farm

B. Battisti, G. Verao Fernandez, G. Giorgi, and P. Troch

Abstract—**The maximization of the power output of an array of wave energy converters (WECs) and its impact on the surrounding area are two fundamental, strictly interconnected, aspects that must be considered in the design of a wave farm. The effect of those two elements combined, usually considered separately, is evaluated, in this study, for a small farm of floating devices. The numerical simulations are performed using a coupled model between the BEM solver Capytaine (near-field solution) and the wave propagation model MILDwave (far-field solution). The farm is located off the coast of Pantelleria Island and is composed of three PeWECs, WECs designed for the Mediterranean Sea. The power output and the perturbed wave field around the PeWEC farm are compared to the single device, for different distances among the WECs. Moreover, a Power Take-Off (PTO) is implemented for assessing the difference in the far-field effects between a controlled and an uncontrolled case. Results show that the wake produced by the PeWEC farm is more prominent and more complex with respect to the single device. The inclusion of the PTO contributes to further attenuate the wave field in the lee of the PeWEC farm.**

Index Terms—**WEC farm, PeWEC, wave energy, coastal protection, Capytaine, MILDwave, far-field effects**

I. Introduction

DIFFERENT kinds of Wave Energy Converter (WEC) at different levels of technology readiness are being developed to extract energy from waves. They all have in common their deployment in farms, as an essential step for wave energy to reach commercial scale and be comparable to other renewable energy sources. Indeed, gathering multiple WECs might stabilize the power output. Additionally, combining together some systems like mooring lines or underwater cables, and sharing the WEC production, installation and maintenance costs, will contribute to decrease the overall cost of energy. [1], [2], among others, determine that the positive interactions created among the WECs in a farm leads to a higher power output than the sum of the power extracted separately by the same amount of devices. Although this result is valid especially for point absorbers and has not been proved for other types of WECs yet, it highlights the enhanced effects of deploying closely spaced devices on the power production and the surrounding wave field. The vast majority of the studies on WEC farms focus on the maximization of the former aspect, the power extraction [3]–[5]. However, the assessment of the impact of a farm on the surrounding marine area is also important for the choice of the installation site and the estimation of the influence on the communities directly linked to such structures [6].

Such a multiobjective study of a WEC farm needs to account for the fluid-structure interactions of every WEC, the WEC-WEC interactions inside the farm and its propagation in the far-field. This diversity of scales and flow dynamics motivates a separation of the domain into subdomains where the most appropriate solver is used for the simulation. Domain decomposition applied to WEC farms is becoming an increasingly widespread practice towards computational cost reduction [7]. For instance, [8], [9] propose a high-fidelity (Computational Fluid Dynamics and Smoothed-Particle Hydrodynamics, respectively) solver for an accurate simulation of the field close to the device and a solver based on potential flow theory for the far-field. The coupling of the two domains is achieved using a buffer zone for a smooth transition between the two different solvers. [10] propose a numerical model coupling the Boundary Element Method (BEM) solver Capytaine [11] for the near-field and the depth-averaged mild-slope equation wave propagation solver MILDwave [12]. Since both methods are based on potential theory, their coupling is straightforward and does not need an intermediate relaxation zone.

We propose here a study on a small WEC farm using the Capytaine-MILDwave coupling methodology. To the best of the authors' knowledge, for the first time in the literature, this study focuses on *both* the productivity *and* the far-field effects of a farm of three converters with respect to a single device case. The case study is a farm of PeWEC (Pendulum Wave Energy Converter) [13], [14], a floating, multidegree of freedom device, developed at Politecnico di Torino, to be installed off the coast of the Pantelleria island, in the trait of Sicily, Italy. Three different regular waves are tested, both for a single device and the farm, with different spacing among the WECs. In addition to the classic assessment of the effect of a farm of passive devices, a Power Take-Off (PTO) is implemented to highlight the importance of considering the active contribution of the converters in extracting power from wave, thus changing the wave field to a greater extent.

The paper is structured as follows. In Sec. II the

This publication is based upon work from COST Action CA17105, supported by COST (European Cooperation in Science and Technology). The project has also received funding from the European Union's Horizon 2020 research and innovation programme under the Marie Skłodowska-Curie grant agreement No: 101068736.

B. Battisti is at the Marine Offshore Renewable Energy Lab, Department of Mechanical and Aerospace Engineering, Politecnico di Torino, Turin, Italy and Université de Bordeaux, IMB, UMR 5251, Talence, France (e-mail: beatrice.battisti@polito.it).

G. Verao Fernandez is at the Department of Built Environment, Aalborg University, Denmark (e-mail: gvf@build.aau.dk).

G. Giorgi is at the Marine Offshore Renewable Energy Lab, Department of Mechanical and Aerospace Engineering, Politecnico di Torino, Turin, Italy (e-mail: giuseppe.giorgi@polito.it).

P. Troch is at the Department of Civil Engineering, Ghent University, Belgium (e-mail: Peter.Troch@UGent.be).

Digital Object Identifier:
https://doi.org/10.36688/ewtec-2023-333

numerical model is shortly described, while the chosen device and the case study are outlined respectively in Sec. III. and Sec. IV; in Sec. V the results of the simulations and some considerations are presented, before the conclusions.

II. Numerical Model

In the numerical model, the dynamics close to the WECs are separated from, and treated differently than the dynamics of the large area surrounding the farm. In this way, the most appropriate solver is applied for the modelling of the wave-structure interaction and the computation of the perturbed wave field in a small domain close to the farm, and another solver is used for the wave propagation in the wide area far from the farm. The procedure is, thus, based on a domain decomposition, as shown in Fig. 1, where Ω_{NF} represents the near-field and Ω_{FF} the far-field (not in scale).

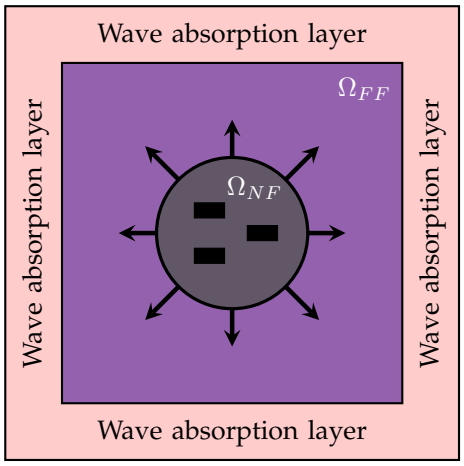

Fig. 1. Outline of the domain decomposition for the one-way coupling methodology, adapted from [10].

The coupling between the two numerical models can, in general, be either one-way or two-way. The difference is the direction of the propagation of the information: in a one-way fashion from Ω_{NF} to Ω_{FF} only, without changes on the inner domain solution; or in both directions, yielding to a solution that is dependent on the two model results. The methodology chosen for this paper is a one-way coupling, where the near-field is first computed in the circular domain Ω_{NF} and then propagated in Ω_{FF}.

Both numerical models rely on linear potential flow theory, namely assuming waves with low steepness and small body displacement. Nonlinearities, such as viscosity and varying wetted surface, are assumed to have little effect on both the dynamics of the floaters and especially on the perturbation of the surrounding wave field; this hypotesis is justified with the relatively small dimension of the floaters with respect to the wavelength. Therefore, the fluid is assumed to be inviscid and incompressible, and the flow irrotational. Thus, defining the spatial variable $\mathbf{x} = (x, y, z)$ and the temporal variable t, there exists a velocity potential $\Phi(\mathbf{x}, t) = \mathrm{Re}[\phi(\mathbf{x})\, \mathrm{e}^{\mathrm{i}\omega t}]$, with ω the angular wave frequency, that allows the fluid velocity to be expressed as its gradient: $\mathbf{u} = \nabla\Phi$. The linearization comes from the assumptions of small amplitude motions of a body inserted in the domain, and small wave amplitudes. As a consequence, the potential of the wave field perturbed by the presence of the body, ϕ^P, can be defined as the superposition of three elements:

$$\phi^P = \phi^I + \phi^D + \mathrm{i}\omega \sum_{q=1}^{n_{DOF}} \phi_q^R. \tag{1}$$

In (1), ϕ^I is the incident potential of a wave of unitary amplitude travelling with a certain direction, ϕ^D is the diffracted potential caused by the presence of the body, and ϕ^R is the radiated potential, due to the motion of the body. In particular, ϕ^R is given by the sum of the n_{DOF} degrees of freedom of the body.

Assuming that the reference system of the domain has the vertical direction positive downwards, with origin on the wave elevation, then the expression of the free surface is obtained as

$$\eta = -\mathrm{i}\,\frac{\omega}{g}\phi\bigg|_{z=0}, \tag{2}$$

where g is the gravity.

A. Wave-structure interaction solver

For the near-field domain Ω_{NF}, the BEM (Boundary Element Method) solver Capytaine [11] is chosen. Capytaine is a Python implementation of NEMOH, developed at Ecole Centrale de Nantes, in France [15]. The results are solution of a boundary value problem, composed by Laplace's equation $\nabla^2\phi = 0$ and a set of boundary conditions on the free surface, the bottom of the domain, the wetted surface of the body, and the far-field area. An additional assumption for the BEM solver is that the seabed is flat, which is considered reasonable since an array normally covers a moderately large area. In addition to the potential of the flow field, Capytaine also calculates the hydrodynamic characteristics of the floating body of n_{DOF} degrees of freedom (DoFs), solving the equation of motion [16]:

$$[-\omega^2(\boldsymbol{M} + \boldsymbol{A}(\omega)) + \mathrm{i}\omega\boldsymbol{B}(\omega) + \boldsymbol{C}]\boldsymbol{\zeta}(\omega) = \boldsymbol{F_{ext}}(\boldsymbol{\omega}), \tag{3}$$

where $\boldsymbol{M}$ is the body mass matrix, defined using the mass of the body, its center of gravity, and the moments of inertia, and ζ are the displacements. $\boldsymbol{A}(\omega)$ is the added mass matrix, $\boldsymbol{B}(\omega)$ the damping matrix, $\boldsymbol{C}$ the matrix of hydrostatic and gravitational restoring coefficients, and $\boldsymbol{F_{ext}}(\omega)$ represents the external excitation forces. For a chosen body, $\boldsymbol{M}$ is known, and $\boldsymbol{A}$, $\boldsymbol{B}$, $\boldsymbol{C}$ and $\boldsymbol{F_{ext}}$ are evaluated by the BEM solver. Moreover, the Response Amplitude Operator (RAO) of the device is computed as:

$$RAO(\omega) = \frac{\boldsymbol{\zeta}}{A_w} = \boldsymbol{f_{ext}}\ \left[-\omega^2(\boldsymbol{M} + \boldsymbol{A}) + \mathrm{i}\omega\boldsymbol{B} + \boldsymbol{C}\right]^{-1}, \tag{4}$$

where A_w is the wave amplitude, and $\boldsymbol{f_{ext}} = \boldsymbol{F_{ext}}/A_w$.

B. Wave propagation solver

In the large domain surrounding the WEC farm, the wave propagation solver MILDwave, developed at the Coastal Engineering Research Group of Ghent University in Belgium [12], is used to solve the mild-slope equation [17]:

$$\nabla \cdot (c\ c_g \nabla \phi) + k^2 c c_g \phi = 0. \tag{5}$$

Here, $k = \frac{2\pi}{\lambda}$ is the angular wave number, with λ the wavelength, c is the phase velocity and c_g the group velocity of the wave. Equation (5) is depth-integrated and solved on a Cartesian mesh for the far-field domain Ω_{FF}, surrounded by absorption zones modelled as sponge layers, to avoid wave reflection. MILDwave is able to account for varying bathymetries, as long as the mild-slope condition is met.

C. Coupling procedure

For the one-way coupling technique, the incident wave field η^I is generated in MILDwave along a linear wave generation boundary and propagated across the domain. The radiated and diffracted wave fields, namely η^R and η^D, are first calculated in Capytaine in the frequency domain. Then, they are transformed into the time domain and propagated in the MILDwave domain using a circular wave generation boundary. Across the boundary, the waves are forced to propagate away from Ω_{NF}. The perturbed wave field MILDwave is obtained as the superposition of two simulations, the incident wave field, and the diffracted and radiated wave fields: $\eta^P = \eta^I + \eta^D + \eta^R$, analogously to (1). The radius of the circular boundary must be big enough to include all the devices of the farm, and its value is chosen to obtain an even distribution of the wave fields on the circumference [18].

III. Device

PeWEC [13] is the device chosen for this study, a rotating mass device characterized by a pendulum inside a floating hull, where energy is extracted from the pitching motion of the hull. It is moored to the seabed by a spreading catenary, that allows it to align the pitch degree of freedom to the incoming waves. Power production is obtained thanks to the relative motion of the pendulum with respect to the shaft of an electrical generator, and it is controlled by a PTO. Fig. 2 shows a simplified outline of the device, and the main characteristics are listed in Table I.

For a fast nonlinear description of the floater, the reader should refer to [19]; for the numerical simulations of this paper, however, a linearized model of the device is implemented. For instance, the effect of the mooring, which is nonlinear, is not taken into account for this study. Moreover, since the working principle of PeWEC is mainly planar, the degrees of freedom under investigation can be reduced to surge, heave and pitch ($n_{DOF} = 3$). Concerning the power transformation, the PTO acts on the rotational degree of freedom of the pendulum, whose displacement is ε (see Fig. 2), yielding to an additional equation to the system, (3). The equation of motion matrices have now dimensions $n_{DOF} + 1$ and are modified to include the coupling of the pendulum and the hull, and the action and reaction effects of the PTO, proportional to the displacement and velocity of the pendulum [13]. The proportionality constants are evaluated as to maximize the power absorption of a single device, defined as in [20]:

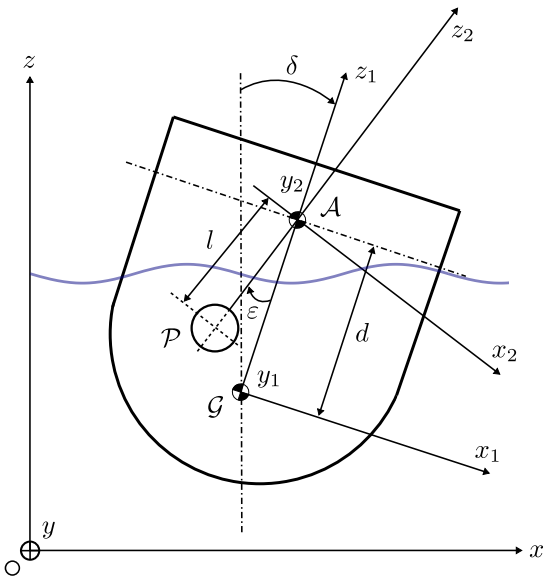

Fig. 2. Schematic representation of the PeWEC device.

TABLE I
Main PeWEC's characteristics

Definition		Value
Hull length		14.8 m
Hull width		22.5 m
Hull height		7.4 m
Hull draft		4.81 m
Hull mass		1118 t
Moments of inertia	along x	5.54×10^7 kg m^2
	along y	2.99×10^7 kg m^2
	along z	7.22×10^7 kg m^2
Resonance period		6.55 s

$$P = \frac{1}{2}\omega^2 \boldsymbol{\zeta}^T \mathrm{B}_{PTO} \boldsymbol{\zeta}^*, \tag{6}$$

where the superscripts ^{T} represents the transpose and * the complex conjugate.
For simplicity, the PTO characteristics are the same for all the devices in the array, and the matrices of (3) have dimensions $n_B \cdot (n_{DOF} + 1)$, with n_B the number of bodies in the farm. The presence of the PTO not only allows power extraction, but also impacts the wave field, since it influences the response of the converters, and thus its radiated field ϕ^R.

IV. Case study

Pantelleria, a small island in the south-west of Italy, is chosen as case study. The installation site of the WEC farm is represented by the red shaded area shown in Fig. 3.

The bathymetry information is retrieved from the European Marine Observation and Data Network

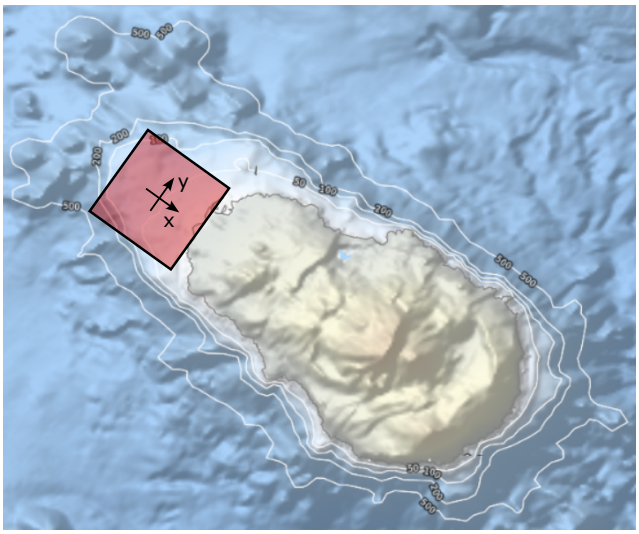

Fig. 3. WEC farm domain (in red) off the coast of Pantelleria island.

(EMODnet) portal [21]. The numerical domain extends for $4\,\mathrm{km}$ in the x-axis and $4\,\mathrm{km}$ in the y-axis. The bathymetrical data is modeled as a slope gently going from an initial depth of $100\,\mathrm{m}$ to $9\,\mathrm{m}$ along the x-axis, and it is assumed constant on the y-axis. The farm is placed at $700\,\mathrm{m}$ from the coast, at a water depth of $30\,\mathrm{m}$.

The wave data are acquired from the ERA5 database of the European Center for Medium-Range Weather Forecasts (ECMRWF) [22] via the MORE-EST Wave and Wind Platform [23], [24] and are referred to the 2010-2019 period. The mean significant wave heights H_s and the mean peak periods T_p are averaged on the seasons, as well as the wave direction δ, thus generating the three representative wave cases listed in Table II.

TABLE II
CHARACTERISTICS OF THE ANALYZED WAVES

Season	H_s	T_p	δ
Winter	1.5m	5.6s	15°
Spring/Autumn	1.1m	5s	10°
Summer	0.7m	4s	0°

It is worth noting that the wave characteristics for Spring and Autumn are condensed in only one wave case, as their values are comparable. The simulated waves are regular and unidirectional, with main direction perpendicular to the coast, and aligned to the main wave direction (North-West) for this site. However, a slight direction deviation δ from the main one is defined for the three different waves, as the most occurring for that season.

V. RESULTS

In this study, one farm layout is considered, with two devices at the front and one at the back, separated by a distance d, as shown in Fig. 4. Taking the PeWEC hull width as the device characteristic length L, two cases are simulated, for $d = 5L$ and $d = 20L$. For the former layout, the devices are expected to interact, considerably impacting the power extraction and the wake behind the array, with respect to the single device. For the latter layout, this influence should be less significant.

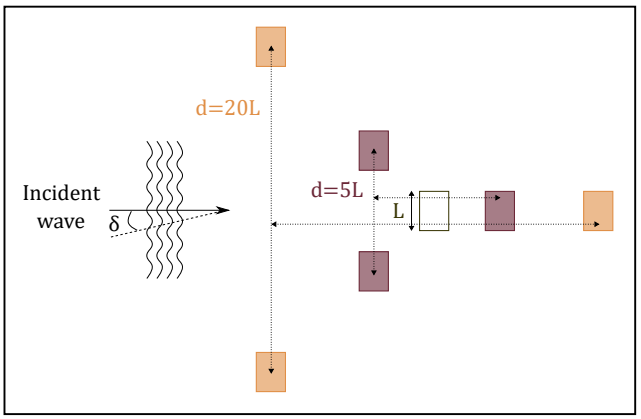

Fig. 4. Outline of the tested cases: a single device, and two 3-WECs farms, for different distances among the devices (not in scale).

As illustrated in Sec. II-C, the coupling methodology entails first the simulation of the near-field with Capytaine. The near-field domain is a $800\,\mathrm{m} \times 800\,\mathrm{m}$ square, as evidenced in Fig. 5, where the wave field, in terms of disturbance coefficient

$$K_d = \eta^P / \eta^I, \tag{7}$$

is plotted for the single device and the two farms, for the case with and without PTO, for the Winter wave case.

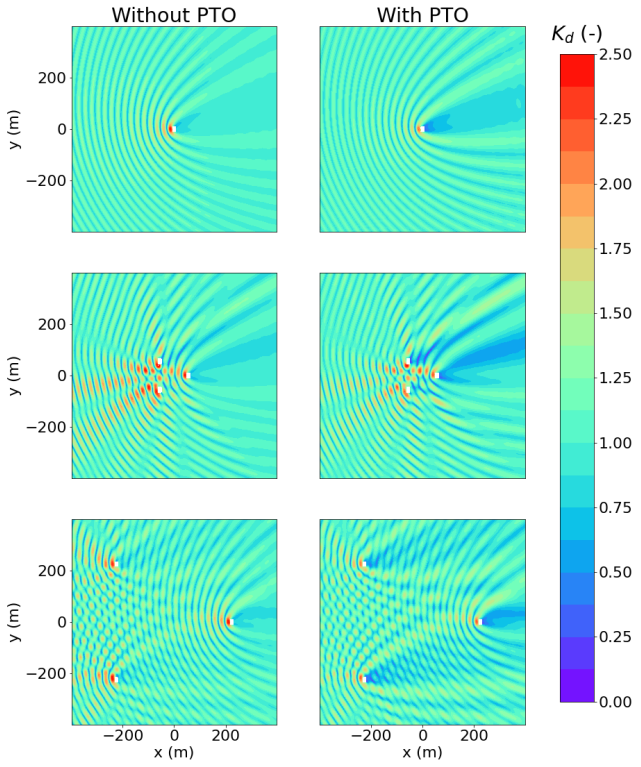

Fig. 5. K_d disturbance coefficient for the near-field, for the Winter wave case. First row: single device; second row: 3-WECs farm, $d = 5L$; third row: 3-WECs farm, $d = 20L$. The color bar is uniformed on all the results for a qualitative comparison.

In Fig. 5, it can be seen how the closer the WECs are located, the more impact have the diffracted and

radiated wave field on the incoming wave field. The wake behind the farm, or the single device, is enhanced in the cases with the PTO, since the PeWEC is actively extracting energy from the waves. Indeed, when the converter is controlled, the extracted power can be evaluated as in (6). To better understand the effect of the farm, the q-factor is defined as:

$$q = \frac{P_a}{n_B\, P_s}, \tag{8}$$

where P_a is the power extracted by the farm, given by the sum of the power of all the devices in the farm, and P_s is the power extracted by a single device. q can have values bigger or smaller than unity, indicating when the farm produces, respectively, more or less than n_B devices considered isolated, and thus, not interacting.

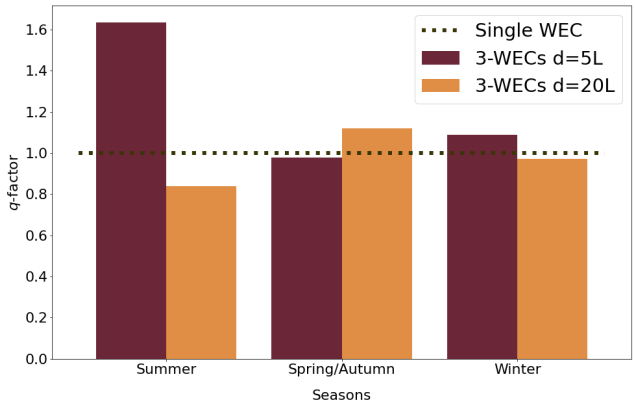

Fig. 6. Comparison of the q-factor of the farms in the different seasons, with respect to the single device.

Fig. 6 shows the productivity of the farms normalized with respect to the single device, for the three different wave cases. In Summer, when the wave is aligned with the array, and the wave field is symmetric, the power extraction of the case $d = 5L$ is more than 50% higher than the power extracted by three isolated devices; for the larger array, however, the interactions are modest and negative, meaning that they decrease the total power production. The two other seasons show different behaviors: when the waves have even a small direction $\delta \neq 0°$, the wave pattern becomes very complex (see Fig. 5), and the interactions do not show a trend in the q-factor fluctuation. It must be noted that the PeWEC is considered here as a 3-DoFs body, that best extracts energy when the pitching direction is aligned with the wave direction. Considering the PeWECs with all the 6-DoFs would change the wave perturbation and the power extraction. Moreover, all the WECs in the farm have the same PTO, independently of their position in the WEC farm with respect to the wave direction, thus providing, in this case, suboptimal control of the WEC farm.

The second part of the coupling methodology is the propagation, with MILDwave, of the information from the near-field domain to the far-field, until, in this case, the coast. The propagation of the wave fields from Fig. 5 are shown in Fig. 7, for the Winter season, with and without PTO.

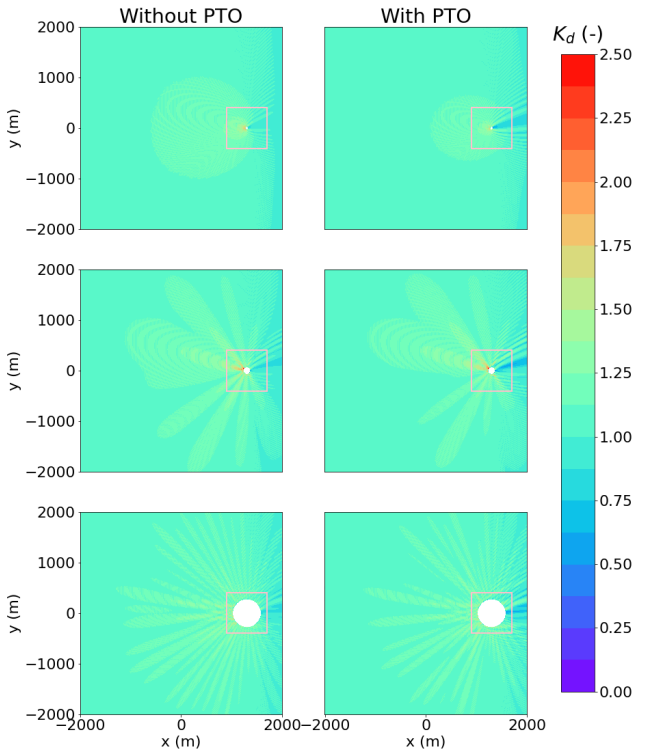

Fig. 7. K_d disturbance coefficient for the far-field, for the Winter wave case. First row: single device; second row: 3-WECs farm, $d = 5L$; third row: 3-WECs farm, $d = 20L$. The color bar is uniformed on all the results for a qualitative comparison. The pink square represents the Capytaine (near-field) simulation domain, the white circle represents the wave generation boundary in MILDwave.

The coast is surely affected by the presence of one or more PeWECs, with a higher effect when the PTO is considered. In Fig. 8, we take the down-wave boundary section of the simulation domain, parallel to the coast of Pantelleria and we trace the variation of the wave elevation, for the three seasons. In Fig. 8a, during Summer, the envelope is symmetric, and the wake is concentrated in the center part, fading away further away from the center. In Spring/Autumn and Winter, due to a $\delta \neq 0°$, the coast is not perpendicular any more to the wave propagation direction, and, thus, the wave profile is quite different, showing unsymmetrical features and an influence spread all over the section, and thus, the coast.

However, in the three wave cases, the K_d is not centered on unity, but it is slightly smaller: this shift is caused by the shoaling effect of the sloping bathymetry. Indeed, the shape of the seabed strongly affects the wave field, and it is important in analyses of large marine area. The combined effect of the farm wake and the shallow water is visible also in Fig. 9, where the disturbance in the wave elevation is plotted in the direction aligned with the wave, for the Summer case. The K_d is unity for a large part of the domain in front of the farm (not shown in the graphs for simplicity), increasing closer to the farm. Behind the farm, the K_d is very small and gently recovers until the coast, but remains smaller than unity.

The effect of the PTO is clear, further decreasing K_d, even if, in this case, the effect is mild, as the PTO is fixed for all the devices. In Table III, the percentage

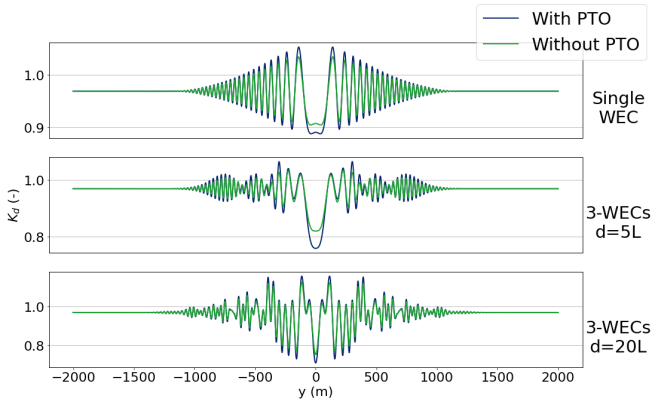

(a) Summer

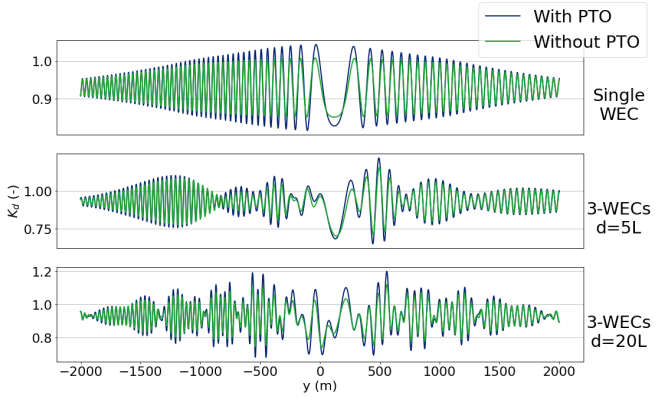

(b) Spring/Autumn

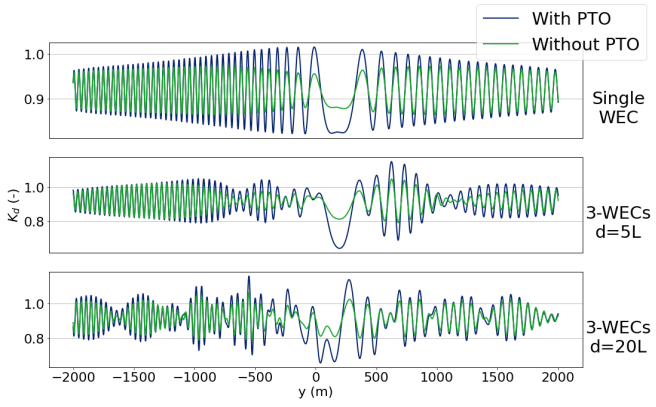

(c) Winter

Fig. 8. K_d disturbance coefficient at the coast, for the different seasons.

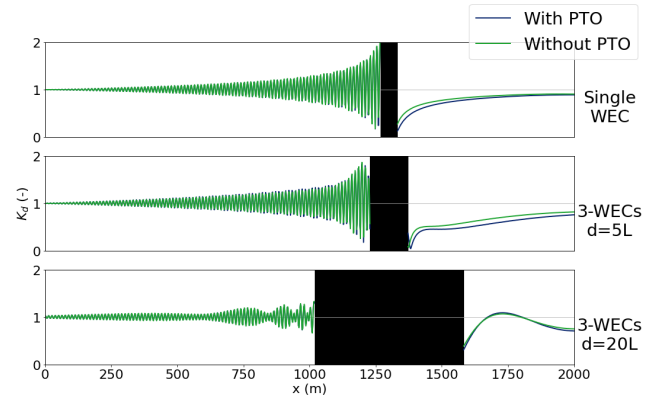

Fig. 9. K_d disturbance coefficient along the wave direction, for the Summer wave case. The black rectangle represents the wave generation boundary in MILDwave, where the solution is not computed.

difference in the K_d for the case with the PTO, compared with the case without the PTO, is evaluated at the coast ($x = 2000\,\mathrm{m}$).

TABLE III
PERCENTAGE VARIATION OF K_d WITH THE PTO

Season	Single Device	3-WECs $d = 5L$	3-WECs $d = 20L$
Winter	-4.93%	-18.75%	-16.81%
Spring/Autumn	-4.17%	-7.41%	-8.07%
Summer	-1.84%	-7.40%	-5.76%

Since the PeWEC is a pitching WEC floating close to the sea surface, with a rounded shape and small diffraction, its attenuation capability is expected to be modest; despite this, Table III still clearly shows that the PTO has a significant impact on the reduction of K_d. On the other hand, a greater impact is expected for diffraction-driven devices, such as Oscillating Surge Wave Energy Converters [25].

VI. CONCLUSION

In the wave energy field, there is the common agreement that devices should be developed in an array configuration in order to be economically viable and to provide a significant contribution to local communities. Two main aspects are often considered: on the one hand, the renewable energy production is the major focus, since ocean power harvesting is renown to have a high potential; on the other hand, it is often argued that a secondary beneficial impact may be achieved for coastal protection, leveraging the fact that energy is withdrawn from the waves, consequently dampening out their effect on the coast. However, such aspects are usually treated separately, hence overlooking potential interactions of such intertwined phenomena.

In this paper, a case study is considered in order to obtain first quantitative results about the potential relevance of such an interplay: a small PeWEC farm is analyzed both in terms of power extraction and the far-field effect, considering the real application scenario of Pantelleria Island in the Strait of Sicily. Results indeed corroborate the need for considering the synergy between the two aspects in the design of a WEC farm, which is beneficial not only for energy production, but also for coastal protection. In fact, considering different layout configurations, it is found that the wave field attenuation can vary from about 2 % up to almost 19%, while the q-factor ranges from 0.8 to 1.6. It is therefore worth of further investigation to analyse how such metrics are dependent on the array layout and control setup, in order to eventually define suitable compromises, according to the specific installation sites.

REFERENCES

[1] B. Borgarino, A. Babarit, and P. Ferrant, "Impact of wave interactions effects on energy absorption in large arrays of wave energy converters," *Ocean Engineering*, vol. 41, pp. 79–88, 2012. [Online]. Available: https://www.sciencedirect.com/science/article/pii/S0029801812000054

[2] C. Sharp and B. DuPont, "Wave energy converter array optimization: A genetic algorithm approach and minimum separation distance study," *Ocean Engineering*, vol. 163, pp. 148–156, 2018. [Online]. Available: https://www.sciencedirect.com/science/article/pii/S0029801818309521

[3] B. F. M. Child and V. Venugopal, "Optimal configurations of wave energy device arrays," *Ocean Engineering*, vol. 37, no. 16, pp. 1402–1417, 2010. [Online]. Available: https://www.sciencedirect.com/science/article/pii/S0029801810001447

[4] S.-H. Yang, J. W. Ringsberg, and E. Johnson, "Wave energy converters in array configurations—influence of interaction effects on the power performance and fatigue of mooring lines," *Ocean Engineering*, vol. 211, p. 107294, 2020. [Online]. Available: https://www.sciencedirect.com/science/article/pii/S0029801820303371

[5] F. Niosi, B. Battisti, and S. A. Sirigu, "Influence of hydrodynamic interactions on the productivity of pewec wave energy converter array," in *2022 International Conference on Electrical, Computer, Communications and Mechatronics Engineering (ICECCME)*, 2022, pp. 1–6.

[6] J. D. Roberts, C. Jones, and J. Magalen, "Wave energy converter (wec) array effects on wave current and sediment circulation: Monterey bay ca." 9 2014. [Online]. Available: https://www.osti.gov/biblio/1156603

[7] J. Davidson and R. Costello, "Efficient nonlinear hydrodynamic models for wave energy converter design—a scoping study," *Journal of Marine Science and Engineering*, vol. 8, no. 1, 2020.

[8] J. Kemper, C. Windt, K. Graf, and J. Ringwood, "Development towards a nested hydrodynamic model for the numerical analysis of ocean wave energy systems," in *Proceedings of the 13th European Wave and Tidal Energy Conference (EWTEC2019)*, 08 2019.

[9] T. Verbrugghe, V. Stratigaki, C. Altomare, J. M. Domínguez, P. Troch, and A. Kortenhaus, "Implementation of open boundaries within a two-way coupled sph model to simulate nonlinear wave–structure interactions," *Energies*, vol. 12, no. 4, 2019.

[10] G. Verao Fernandez, P. Balitsky, V. Stratigaki, and P. Troch, "Coupling methodology for studying the far field effects of wave energy converter arrays over a varying bathymetry," *Energies*, vol. 11, no. 11, 2018.

[11] M. Ancellin and F. Dias, "Capytaine: a Python-based linear potential flow solver," *Journal of Open Source Software*, vol. 4, no. 36, p. 1341, apr 2019. [Online]. Available: https://doi.org/10.21105%2Fjoss.01341

[12] P. Troch, "Mildwave – a numerical model for propagation and transformation of linear water waves," Department of Civil Engineering, Ghent University, Internal Report, 1998.

[13] S. A. Sirigu, L. Foglietta, G. Giorgi, M. Bonfanti, G. Cervelli, G. Bracco, and G. Mattiazzo, "Techno-economic optimisation for a wave energy converter via genetic algorithm," *Journal of Marine Science and Engineering*, vol. 8, no. 7, 2020. [Online]. Available: https://www.mdpi.com/2077-1312/8/7/482

[14] F. Carapellese, E. Pasta, B. Paduano, N. Faedo, and G. Mattiazzo, "Intuitive lti energy-maximising control design for wave energy converters: the pewec case," *Ocean Engineering*, vol. 256, 05 2022.

[15] A. Babarit and G. Delhommeau, "Theoretical and numerical aspects of the open source BEM solver NEMOH," in *Proceedings of the 11th European Wave and Tidal Energy Conference (EWTEC2015)*, Nantes, France, 2015.

[16] J. N. Newman, *Marine hydrodynamics*. MIT Press Cambridge, 1977.

[17] M. W. Dingemans, "Water wave propagation over uneven bottoms," Ph.D. dissertation, TU Delft, 1994.

[18] P. Balitsky, G. Verao Fernandez, V. Stratigaki, and P. Troch, "Coupling methodology for modelling the near-field and far-field effects of a wave energy converter," in *Proceedings of the 36th International Conference on Ocean, Arctic and Offshore Engineering (OMAE2017)*, Trondheim, Norway, 06 2017.

[19] G. Giorgi, S. Sirigu, M. Bonfanti, G. Bracco, and G. Mattiazzo, "Fast nonlinear froude–krylov force calculation for prismatic floating platforms: a wave energy conversion application case," *Journal of Ocean Engineering and Marine Energy*, vol. 7, pp. 1–19, 11 2021.

[20] M. Folley, Ed., *Numerical modelling of wave energy converters*. Elsevier Ltd, 2016.

[21] EMODnet Bathymetry portal. [Online]. Available: https://www.emodnet-bathymetry.eu

[22] G. Cervelli, L. Parrinello, C. Moscoloni, and G. Giorgi, "Comparison of the ERA5 Wave Forecasting Dataset against Buoy Record," *Instrumentation Mesure Metrologie*, vol. 21, no. 3, pp. 87–95, 2022.

[23] (2022) More-est platform. MOREnergyLab. [Online]. Available: http://www.morenergylab.polito.it/more-est-platform/

[24] G. Giorgi, R. Novo, G. Cervelli, and G. Bracco, "Wave energy converters technology database for a web-based platform for evaluating wave energy resource and productivity potential," in *Proceedings of the 5th International Conference on Renewable Energies Offshore (RENEW 2022)*, 10 2022, pp. 33–41.

[25] G. Verao Fernandez, P. Balitsky, N. Tomey Bozo, V. Stratigaki, and P. Troch, "Far-field effects by arrays of oscillating wave surge converters and heaving point absorbers: a comparative study," in *Proceedings of the 12th European Wave and Tidal Energy Conference (EWTEC2017)*, 09 2017.